

Particle captured by a field-modulating vortex through dielectrophoresis force

Bing Yan(严兵), Bo Chen(陈波), Zerui Peng(彭泽瑞), and Yong-Liang Xiong(熊永亮)
Citation: Chin. Phys. B, 2022, 31 (**3**): 034703. DOI: 10.1088/1674-1056/ac248a
Journal homepage: http://cpb.iphy.ac.cn; http://iopscience.iop.org/cpb

What follows is a list of articles you may be interested in

Effect of Joule heating on the electroosmotic microvortex and dielectrophoretic particle separation controlled by local electric field

Bing Yan(严兵), Bo Chen(陈波), Yongliang Xiong(熊永亮), and Zerui Peng(彭泽瑞)
Chin. Phys. B, 2021, 30 (**11**): 114701. DOI: 10.1088/1674-1056/abf108

Non-Stokes drag coefficient in single-particle electrophoresis:New insights on a classical problem

Mai-Jia Liao(廖麦嘉), Ming-Tzo Wei(魏名佐), Shi-Xin Xu(徐士鑫), H Daniel Ou-Yang(歐陽新喬), Ping Sheng(沈平)
Chin. Phys. B, 2019, 28 (**8**): 084701. DOI: 10.1088/1674-1056/28/8/084701

Development of a new correlation to calculate permeability for flows with high Knudsen number

Esmaeil Dehdashti
Chin. Phys. B, 2016, 25 (**2**): 024702. DOI: 10.1088/1674-1056/25/2/024702

Simulation of fluid-structure interaction in a microchannel using the lattice Boltzmann method and size-dependent beam element on a graphics processing unit

Vahid Esfahanian, Esmaeil Dehdashti, Amir Mehdi Dehrouye-Semnani
Chin. Phys. B, 2014, 23 (**8**): 084702. DOI: 10.1088/1674-1056/23/8/084702

Molecular dynamics simulations of the nano-droplet impact process on hydrophobic surfaces

Hu Hai-Bao, Chen Li-Bin, Bao Lu-Yao, Huang Su-He
Chin. Phys. B, 2014, 23 (**7**): 074702. DOI: 10.1088/1674-1056/23/7/074702

Particle captured by a field-modulating vortex through dielectrophoresis force

Bing Yan(严兵), Bo Chen(陈波)[†], Zerui Peng(彭泽瑞)[‡], and Yong-Liang Xiong(熊永亮)

School of Aerospace Engineering, Huazhong University of Science and Technology, Wuhan 430074, *China*

(Received 2 July 2021; revised manuscript received 18 August 2021; accepted manuscript online 8 September 2021)

In microfluidic technology, dielectrophoresis (DEP) is commonly used to manipulate particles. In this work, the fluid–particle interactions in a microfluidic system are investigated numerically by a finite difference method (FDM) for electric field distribution and a lattice Boltzmann method (LBM) for the fluid flow. In this system, efficient particle manipulation may be realized by combining DEP and field-modulating vortex. The influence of the density ($\rho_{\rm p}$), radius (r), and initial position of the particle in the y direction ($y_{\rm p0}$), and the slip velocity (u_0) on the particle manipulation are studied systematically. It is found that compared with the particle without action of DEP force, the particle subjected to a DEP force may be captured by the vortex over a wider range of parameters. In the y direction, as $\rho_{\rm p}$ or r increases, the particle can be captured more easily by the vortex since it is subjected to a stronger DEP force. When u_0 is low, particle is more likely to be captured due to the vortex–particle interaction. Furthermore, the flow field around the particle is analyzed to explore the underlying mechanism. The results obtained in the present study may provide theoretical support for engineering applications of field-controlled vortices to manipulate particles.

Keywords: field-modulating vortex, dielectrophoresis, fluid–particle interactions

PACS: 47.57.jd, 47.61.–k, 47.15.Rq **DOI:** 10.1088/1674-1056/ac248a

1. Introduction

Lab-on-a-chip (LOC) technology, and its advantages of portability and integration, have attracted a lot of attention. The LOC can integrate expensive and large-volume laboratory instruments on a tiny chip without sacrificing performance. It can implement a multifunction process by integrating many components, such as sample pretreatment, sample transportation, particles manipulation, the detection and analysis of on-chip reactions and consequences, *etc*.[1] Particle manipulation is a key process that can affect detection accuracy. Dielectrophoresis (DEP) is commonly used for particle manipulation, and it has unique advantages in many respects, such as low cost, fast speed, high efficiency, high sensitivity, excellent controllability, *etc*.

In DEP, particles are suspended and subjected to a net force due to the polarization of an uneven electric field and the generation of relative motion. The electric field gradient is an important factor for DEP performance. Pure DEP technologies are divided into the microelectrode-based DEP (eDEP) and insulator-based DEP (iDEP). In the early stages, eDEP was widely used to manipulate particles in a microfluidic system because the system could utilize low voltages, small electrode volume, and electrodes of any shape.[2] According to the arrangements of microelectrodes embedded within microchannel, eDEPs are divided into planar electrodes (2D eDEP) (here, 2D is an abbreviation for two-dimensional), multilayered electrodes (3D eDEP) (here, 3D is an abbreviation for three-dimensional), and microarray dot electrodes.[3] Thin-film 2D electrodes produced with a simple manufacturing process could meet the requirements of DEP and manipulate particles.[4–6] In a 3D eDEP system, the DEP force generated among the multilayered electrodes was used to manipulate target particles.[7–9,11] Standard photolithographic technologies were used to fabricate microarray dot electrodes,[3] which generate a DEP force that can be used to manipulate particles.[12] However, the eDEP has a narrow control range, so its efficiency is low. To address this, researchers have embedded insulating posts in channels to amplify the working region of the DEP. This approach is called iDEP, and is widely used to manipulate the particles and cells.[13–16] However, when high voltages are used in an iDEP system, temperature inside the device increases to a high level due to Joule heating. Since pure DEP technology has its own shortcoming, many researchers have also combined DEP with other microfluidic technologies to manipulate particles, such as the hybrid dielectrophoresis-inertial method,[17] combining DEP with deterministic lateral displacement,[18] combining DEP and electroosmotic micro-vortex,[19–22] and other approaches. These combined technologies can not only make full use of the advantages of pure DEP technology, but also avoid their shortcomings.

When particles move in the vortices, the influence of vortices on particles depends on the parameters of the particles, such as their sizes[23,24] and densities,[25] as well as the properties of the fluid. In the microfluidic technology, it has also

[†]Corresponding author. E-mail: chbo76@hust.edu.cn
[‡]Corresponding author. E-mail: zeruipeng@hust.edu.cn

© 2022 Chinese Physical Society and IOP Publishing Ltd

been found that the orbit of a particle in a vortex is related to the size of that particle.[26,27] Small particles move in the outer orbits, while large ones travel along the inner orbits nearer to the vortex center.[28,29] Shen *et al.*[30,31] found that the orbit of a particle varies with size, density, and inlet Reynolds number, and observed that the area of the orbit of small particles is smaller than that of large particles. Haddadi and Di Carlo[32] studied the interaction between vortex flow and neutrally buoyant spherical particles in channels, and corroborated that the particles of a limited size spiral toward a unique limit cycle orbit. Further, this spiraling flow generates exchanges of fluid mass between the main flow and the vortex flow. Moreover, researchers also found that the motion of a particle differs from tracers that follow streamlines in practical applications, as the presence of a finite size particle can disturb the surrounding fluid flow.[33] However, there are few studies on the combined dielectrophoresis or field-modulating vortex manipulation of particles. In addition, most of the researches are only limited to the influence of the flow field on the particles, ignoring the influence of the particles on the flow field. In this paper, the fluid–particle interactions in a microfluidic system, where the efficient particle manipulation is realized by combining DEP and field-modulating vortex, are investigated numerically by a finite difference method (FDM) for electric field distribution and a lattice Boltzmann method (LBM) for the fluid flow. The influence of the density, diameter and initial position of the particle, and the velocity of the fluid flow on the dynamics of the system are studied systematically. The movement of particle and the capture of particle by vortex in the presence of nDEP force are compared with those in the absence of nDEP force, and the mechanism of field-modulating vortex and DEP combined to manipulate particles is analyzed. Furthermore, the flow field around the particle is analyzed to explore the underlying mechanism. The results obtained in the work may provide theoretical support for engineering applications of field-controlled vortices to manipulate particles.

2. Mathematical model

In this work, electroosmotic flow appears in a channel, full of electrolyte solution, after an external electric field has been applied along it. When a modulating electrode is embedded on the channel wall, slip velocity is used to disturb local flow field, and thus generating a vortex. Because the aspect ratio of the cross-section is large, the fluid flow in the channel can be approximately regarded as a 2D flow between parallel plates.[34,35] The 2D geometrical model is shown in Fig. 1. The corresponding characteristic constants are input as follows: the width of the channel $H = 100$ μm, and the length of the main channel $L_c = 5H = 500$ μm. A modulating electrode $L_e = 1/10L_c$ is used to generate the modulating field.

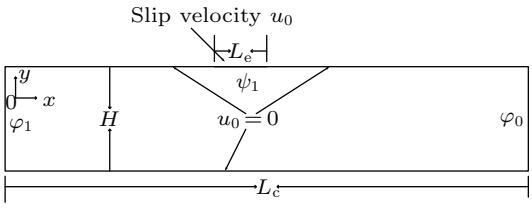


Fig. 1. Geometry of the 2D model.

2.1. Governing equation of electric fields

The electric field contains two parts: the driving electric field and modulating electric field. A driving electric field is generated when the electrodes are located on the inlet part and on the outer part, respectively as shown in Fig. 1, and the electric potentials are appointed to φ_1 and $\varphi_0 = 0$. The driving field is governed by the Laplace equation as follows:[36]

$$\nabla^2 \varphi = 0. \tag{1}$$

The modulating electric field ψ in the field-modulated electric double layer is related to the net charge density ρ_e following the Poisson equation as given below:[36]

$$\varepsilon_f \nabla^2 \psi = -\rho_e, \tag{2}$$

$$\rho_e = ze(n^+ - n^-), \tag{3}$$

$$n^+ = n_0 \mathrm{e}^{-(ze\psi/k_B T)}, \quad n^- = n_0 \mathrm{e}^{(ze\psi/k_B T)}, \tag{4}$$

where ε_f is the permittivity of the electrolyte. e and z are respectively the elementary charge and the valence of the ions ($|z^+| = |z^-| = z$) for the symmetric solution). n^+ and n^- represent the concentrations of the positive and negative ions, respectively. Here, $n_0 = CN_a$ denotes the ion number concentration of the solution, where C is the molar concentration of ions, and the Avogadro number is $N_a = 6.022 \times 10^{23}$. In addition, the Boltzmann constant is $k_B = 1.380 \times 10^{-23}$ J/K. The corresponding boundary condition is $\psi = \psi_1$ for the modulating electrodes, but for the remaining walls, the boundary conditions are $\partial\psi/\partial n = 0$.

2.2. Governing equation of flow field

In this work, the fluid is considered as incompressible and viscous, and the continuity equation and the Navier–Stokes equation are expressed as

$$\nabla \cdot \boldsymbol{U} = 0, \tag{5}$$

$$\rho\left(\frac{\partial \boldsymbol{U}}{\partial t} + (\boldsymbol{U}\cdot\nabla)\boldsymbol{U}\right) = -\nabla P + \mu\nabla^2 \boldsymbol{U}, \tag{6}$$

respectively, where ρ and μ denote the density and viscosity of the fluid, respectively. $\boldsymbol{U}$ represents the velocity vector of the flow field, and P is pressure. The boundary conditions are $p = 0$ for both the inlet and the outlet. For the channel wall, the slip velocity $\boldsymbol{U} = \boldsymbol{U}_0 = -\varepsilon E\psi/\mu$ is applied to the modulating electrode, and for remaining walls, $\boldsymbol{U}_0 = 0$, where E is the electric field strength.

2.3. Governing equation of particle motion

The particle motion obeys Newton's second law, and it is subjected to DEP force $\boldsymbol{F}_{\rm dep}$ and the hydrodynamic force $\boldsymbol{F}_{\rm d}$. Thus, the governing equation is given as follows:

$$m_{\rm p}\frac{{\rm d}^2\boldsymbol{r}_{\rm p}}{{\rm d}t^2}=\boldsymbol{F}_{\rm dep}+\boldsymbol{F}_{\rm d}, \tag{7}$$

where $m_{\rm p}$ is the mass of particles, and $\boldsymbol{r}_{\rm p}$ is the position vector of the particle. The DEP force $\boldsymbol{F}_{\rm dep}$ on a spherical particle is defined as[37]

$$\boldsymbol{F}_{\rm dep}=2\pi r^3\varepsilon_{\rm f}{\rm Re}[f_{\rm cm}]\nabla|\boldsymbol{E}|^2, \tag{8}$$

where r denotes the radius of this particle, and ${\rm Re}[f_{\rm cm}]$ represents taking the real part. In addition, $f_{\rm cm}=(\sigma_{\rm p}-\sigma_{\rm f})/(\sigma_{\rm p}+2\sigma_{\rm f})$ is the Clausius–Mossotti factor for the direct current (DC) electric field, where $\sigma_{\rm f}$ denotes the conductivity of solution, and $\sigma_{\rm p}$ is the conductivity of the particle. The particle is spherical, solid and uniform, and the conductivity of the particle is $\sigma_{\rm p}=\sigma_{\rm p,bulk}+2K_{\rm s}/r$, where $\sigma_{\rm p,bulk}$ is the bulk conductivity, which is approximately zero for polystyrene dielectric particles, and $K_{\rm s}$ is surface conductance, which is changed from 0.2 nS to 2.1 nS.[38]

When a solid particle moves, a momentum exchange occurs between this particle and the flow field. Thus, momentum exchange is used to calculate the hydrodynamic force $F_{\rm d}$. The detailed process of the momentum exchange method is described in the next section.

3. Numerical method

In this work, the fluid–particle interactions in a microfluidic system are investigated numerically by an FDM for electric field distribution and an LBM for the fluid flow. A uniform mesh is used for the numerical solutions of the abovementioned equations, in which the solution domain is represented by s series of cells of size h.

3.1. Solution of electric field by FDM

To obtain the distribution of the electric field across microchannels, the finite difference method is used to solve the Laplace equation and the Poisson–Boltzmann equation. Thus, an over-relaxed iterative scheme is applied, and iterative solutions continue until their convergences. The corresponding equations are given as follows:

$$\begin{aligned} g(i,j)^{(k+1)} &= g(i,j)^{(k)}+\gamma/4[g(i-1,j)^{(k+1)} \\ &\quad +g(i,j-1)^{(k+1)}+g(i+1,j)^{(k)} \\ &\quad +g(i,j+1)^{(k)}-4\times g(i,j)^{(k+1)} \\ &\quad +h^2\times G(i,j)^{(k+1)}], \end{aligned} \tag{9}$$

$$\tau_1 = g(i,j)^{(k+1)}-g(i,j)^{(k)}, \tag{10}$$

$$\tau_2 = \tau_1/g(i,j)^{(k)}, \tag{11}$$

where $g(i,j)$ represents the electric voltage $\varphi(i,j)$ or $\psi(i,j)$, k is the number of iterations, and γ is the over-relaxation factor, which ranges from 0 to 2. Here, if the notation $G(i,j)$ equals 0, equation (9) is used to solve the Laplace equation. When equation (9) is used to solve the Poisson–Boltzmann equation, the notation $G(i,j)$ is equal to $-\rho_{\rm e}/\varepsilon$. The τ_1 and τ_2 are absolute error and relative error, respectively. When the absolute error and relative error are both small enough, the results are considered to be convergent.

3.2. Solution of flow field by LBM

The lattice Bhatnagar–Gross–Krook (LBGK) model is the most widely used in LBM, which can function with a single time step and does not require internal iterations. Thus, the lattice Boltzmann equation[39] is employed in the present simulation, *i.e.*,

$$f_\alpha(\boldsymbol{x}+\boldsymbol{e}_\alpha\Delta t,t+\Delta t)-f_\alpha(\boldsymbol{x},t)=-\frac{1}{\tau}\left[f_\alpha-f_\alpha^{\rm eq}\right], \tag{12}$$

where f_α is the distribution function, and $f_\alpha^{\rm eq}$ is the equilibrium distribution function. $\boldsymbol{x}$ is the position vector, and t is the time. The velocity is discretized into $\boldsymbol{e}_\alpha$ ($\alpha=0$–8) in D2Q9 model, and τ is the relaxation time. The density ρ and the velocity $\boldsymbol{U}$ can be calculated from

$$\rho=\sum_\alpha f_\alpha, \tag{13}$$

$$\boldsymbol{U}=\sum_\alpha f_\alpha\boldsymbol{e}_\alpha/\rho. \tag{14}$$

For a straight microchannel wall, bounce–back conditions are adopted.[40] After completing the stream steps, for the boundary $y=0$, the corresponding boundary conditions are implemented, including $f_2=f_4$, $f_5=f_7$, and $f_6=f_8$. For the boundary $y=H$, the slip velocity $u=u_0$ is applied to the modulating electrode, with the remainder of the boundary at $f_4=f_2$, $f_7=f_5$, and $f_8=f_6$. For a moving curved boundary, the treatment proposed by Lallemand and Luo[41] is adopted, namely, an extension based on the combined method of bounce–back and interpolations is used to treat the curved boundaries.[42]

3.3. Momentum exchange between particle and flow field

The method of momentum exchange is based on the bounce–back scheme. After the collision step is completed, the solid wall can obtain the momentum from the fluid node. At the same time, the fluid node can also obtain momentum by bouncing from the solid node.[39,43] Thus, along this direction, the hydrodynamic force on a solid boundary node at time t is given as

$$\boldsymbol{F}(x_{\rm b})=\left[f_{\bar{\alpha}}(x_{\rm b},t)+f_\alpha(x_{\rm f},t_+)\right]\boldsymbol{e}_\alpha, \tag{15}$$

where t_+ is the post collision time, x_f is the position of the fluid node, and x_b is the position of solid node. Therefore, the total hydrodynamic force on the particle $\boldsymbol{F}_d$ is given by

$$\boldsymbol{F}_d = \sum \boldsymbol{F}(x_b). \tag{16}$$

4. Results and discussion

In this paper, an aqueous solution of potassium chloride at temperature $T = 293$ K is taken as a working solution. The corresponding properties of the fluid are density $\rho = 1000$ kg/m^3, viscosity $\mu = 10^{-3}$ Pa·s, and permittivity $\varepsilon_f = 78\varepsilon_0$, where $\varepsilon_0 = 8.85 \times 10^{-12}$ F/m denotes vacuum permittivity.[38] A solid spherical particle is the goal particle. Grid independence is analyzed by studying the trajectories of a particle under different grid distributions as shown in Fig. 2. Finally, a grid distribution of 1000×200 is selected. The simulation results are expressed in the dimensionless form. For the specific functioning of the dimensionless model, please refer to Appendix A.

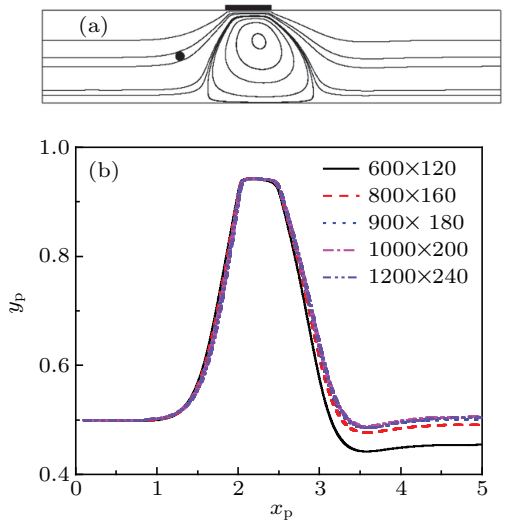


Fig. 2. (a) Schematic diagram of particle motion and (b) trajectories of a particle with different grid distributions, with x_p denoting the position of particle center in x direction, and y_p representing the position of particle center in y direction.

4.1. Model validation

To validate the numerical results, the profiles of the electric field and the flow field obtained by different methods are compared. When a modulating electric field is $\psi_1 = -2$, a cross section at the head of the modulating electrode is selected, and the distribution of the modulating electric field on this cross section is compared as shown in Fig. 3. The results are similar to those calculated by COMSOL. When the slip velocity is $u_0 = 2 \times 10^{-2}$, the flow field is obtained by using different methods as shown in Fig. 4. The forces on this particle, obtained by different methods, are validated, when this particle moves near to the modulating electrode. As shown in Fig. 5, the changes of the forces with their locations are similar, but their magnitudes are different. This is because only the effects of the flow field on the particle are considered by using the COMSOL calculation, and the influence of this particle on the flow field is ignored. In the current method in which the FDM is combined with the LBM, the interaction between the particle and the flow field is considered. Moreover, the DEP force exerted on this particle in the x direction is small, and can be neglected. In this work, the movement of this particle in the y direction is mainly studied.

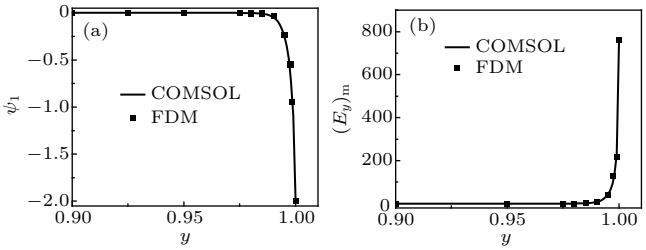


Fig. 3. (a) Distribution of modulating electric voltage ψ_1, and (b) distribution of modulating electric field intensity $(E_y)_m$.

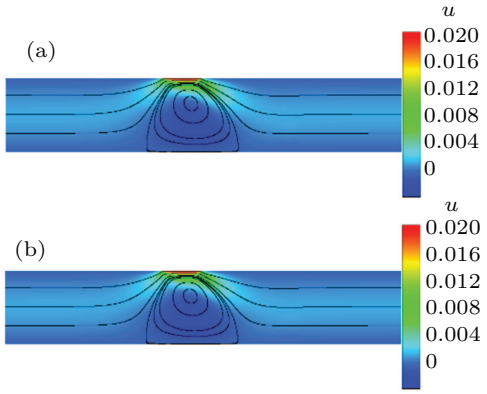


Fig. 4. Schematic diagram of flow field obtained with (a) COMSOL, and (b) LBM.

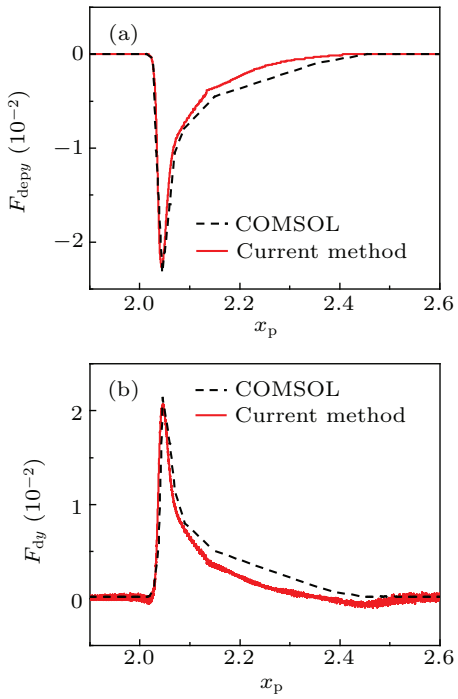


Fig. 5. Variations of (a) DEP force F_{dep}, and (b) hydrodynamic force F_d with location x_p.

4.2. Comparison between results with and without DEP force

When the slip velocity is $u_0 = 2 \times 10^{-2}$, a flow field is produced as shown in Fig. 2(a). The vortex is generated around the modulating electrode due to the disturbance of local flow field. When a particle with a radius of 5 μm is released from the initial position $y_p = 0.5$, it moves with the fluid within the channel. This particle is carried downstream of the channel when it is not subjected to a DEP force as shown in Fig. 6(a). Since there is only a weakly repulsive effect, it can move closer to the wall as it decelerates as shown in Fig. 6(b). However, when a negative DEP (nDEP) force is exerted on this particle, it cannot approach to the modulating electrode due to the strong repulsive effects of the nDEP force, and is eventually pushed into the vortex. Its trajectory first drops sharply and then smooths out as this particle is pushed away from the modulating electrode by the nDEP force, because the net force on the particle varies with its position. Since the nDEP force F_{dep} is active and the hydrodynamic force F_d is passive, F_d varies with F_{dep}. According to Eq. (8), F_{dep} is related to the gradient of the square of strength of the electric field, which means that F_{dep} is related to the distance between this particle and the modulating electrode. A particle moves near the modulating electrode and as this particle approaches to the modulating electrode, F_{depy} is enhanced as shown in Fig. 7(a). When it is away from the modulating electrode, F_{depy} decreases. Meanwhile, F_{dy} also changes in a similar way to F_{depy} as shown in Fig. 7(b), but their functions are opposite. Since the net force F_y is equal to the sum of F_{depy} and F_{dy}, its variation can reflect strength between the two forces. As seen in Fig. 7(c). When F_{depy} exceeds F_{dy}, F_y is negative. On the contrary, F_y is positive as F_{depy} is less than F_{dy}. When the F_y is equal to 0, it moves with the fluid flow.

As a particle moves with the fluid, an interaction occurs between the particle and the flow field. As a hydrodynamic force on this particle is obtained through momentum transfer with the flow field, the flow field is also subjected to the same magnitude and opposite force. To study this effect, a streamline that is formed at the same location of the channel inlet is selected as shown in Fig. 8, and the variation in the streamline is used to describe the effect. Since the hydrodynamic force varies with the position of the particle, the effects of the particle on the flow field change with its position. As it moves near the head of the modulating electrode ($x_p \approx 2.07$), as figure 9(b) shows, the variation in the flow field is significant because the hydrodynamic force is greater ($F_{dy} \approx 2.1 \times 10^{-2}$). As it moves to the center of the modulating electrode ($x_p \approx 2.27$), as illustrated in Fig. 9(c), the hydrodynamic force decreases ($F_{dy} \approx 0.2 \times 10^{-2}$), so the variation in the flow field is weak. As it continues to move downstream ($x_p \approx 2.4$), as shown in Fig. 9(d), there is little variation in the flow field because the force decreases to $F_{dy} \approx 0$. Accordingly, the hydrodynamic force on a particle is stronger, which means that the interaction between this particle and the flow field is stronger, and the influence of the particle on the flow field is more significant.

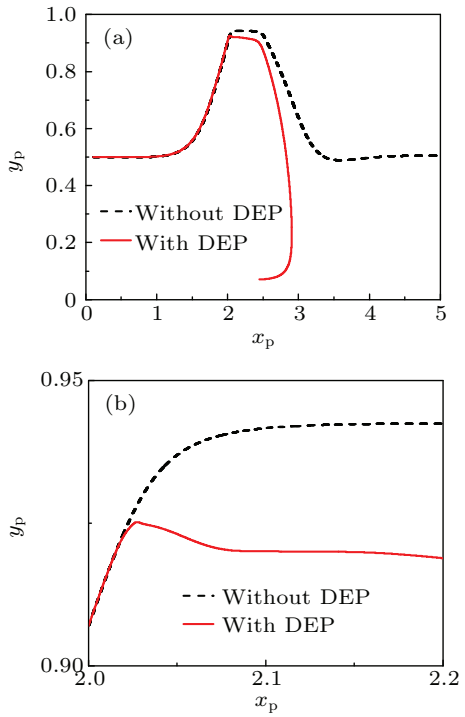


Fig. 6. Schematic diagram of (a) trajectories in different conditions as particle moves within channel, and (b) local trajectories when particle moves near the head of modulating electrode.

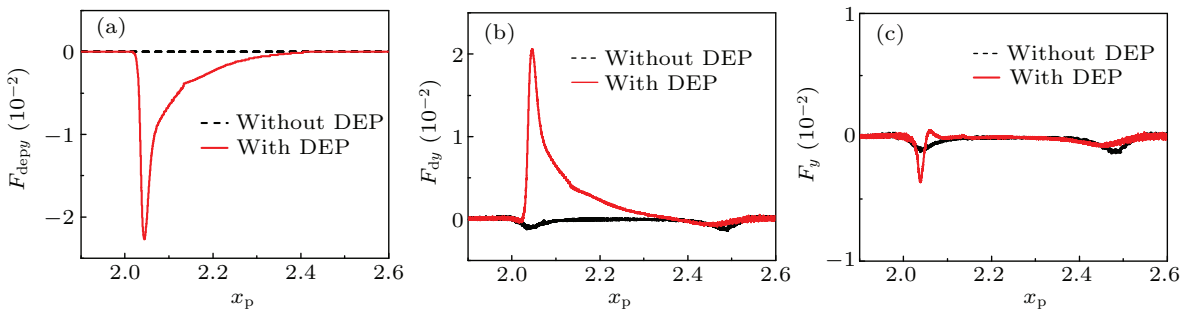


Fig. 7. Variation of (a) DEP force F_{depy}, (b) hydrodynamic force F_{dy}, and (c) net force F_y on particle with its position as it moves near to modulating electrode.

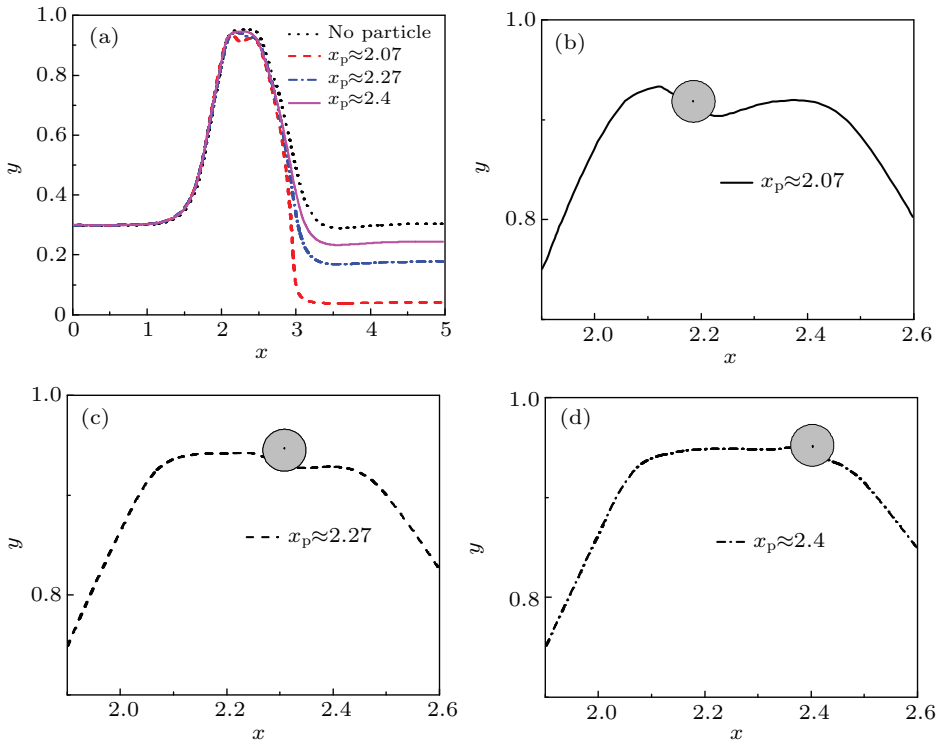


Fig. 8. Schematic diagram of flow field as the particle moves within channel, showing (a) variation of streamlines at the same location, with particle at different positions. and variation of streamline, with this particle at $x_p \approx 2.07$ (b), 2.27 (c), and 2.4 (d).

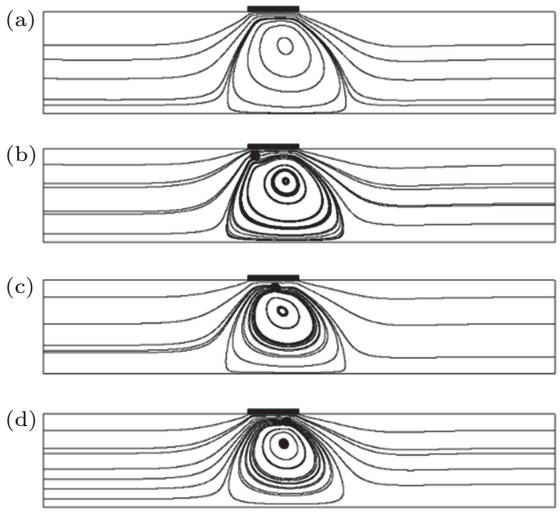


Fig. 9. Schematic diagram of flow field in different conditions for (a) no particle moving with fluid flow, and particle moving to $x_p \approx 2.07$ (b), 2.27 (c), and 2.4 (d).

4.3. Effect of initial position of particle

When the slip velocity is $u_0 = 2 \times 10^{-2}$, a particle with a radius of 5 μm is released from a different initial position y_p. Its motion varies with the y_p when it moves with the fluid. As shown in Fig. 10(a), when the particle is not subjected to an nDEP force, it is released from the initial position $y_p = 0.125$. As it moves near to the modulating electrode, it is closer to the vortex and carried into the vortex. As the q_y increases, this particle is closer to the wall and away from the vortex, finally, it is carried downstream of the channel. When an nDEP force is exerted on this particle, it is also captured by the vortex when its initial position is $y_p = 0.125$ as indicated in Fig. 10(b).

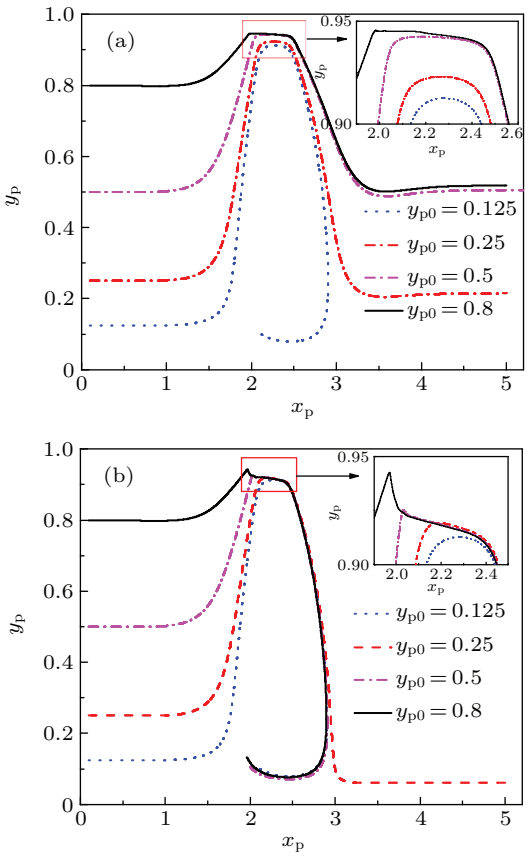


Fig. 10. A particle is released from different initial positions y_{p0}, (a) its trajectories within channel when it is not subjected to an nDEP force, and (b) its trajectories under action of an nDEP force.

Moreover, as it is released from the $y_p = 0.5$ and 0.8, the particle is pushed into the vortex by a strong nDEP force. Since it moves closer to the modulating electrode as y_p in-

creases, the distance between the particle and the modulating electrode is shorter. The maximum value of its location in the y direction $(y_p)_{max}$ increases with y_p increasing as shown in Fig. 11(a). Therefore, the maximum absolute value of the DEP force $|(F_{depy})|_{max}$ on this particle is enhanced as y_p increases as seen in Fig. 11(b), and the maximum absolute value of the hydrodynamic force $|(F_{dy})|_{max}$ and the net force $|(F_y)|_{max}$ on this particle are also enhanced. Accordingly, the particle is more likely to be trapped by the vortex as it is released from a higher y_p. Further, when this particle is subjected to the nDEP force, it is captured more easily by the vortex as $y_{p0} \geq 0.4$.

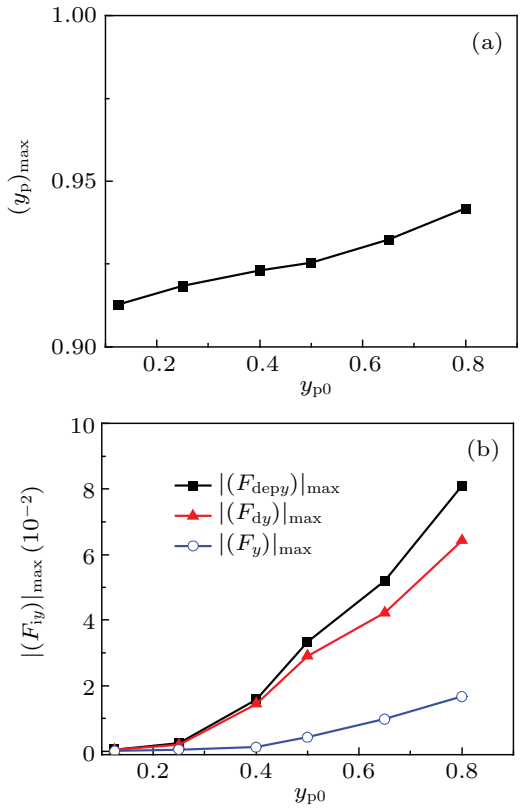


Fig. 11. Variations of (a) maximum position $(y_p)_{max}$ and (b) maximum absolute value of forces $|(F_{iy})|_{max}$ exerted on particle with the initial position y_{p0}.

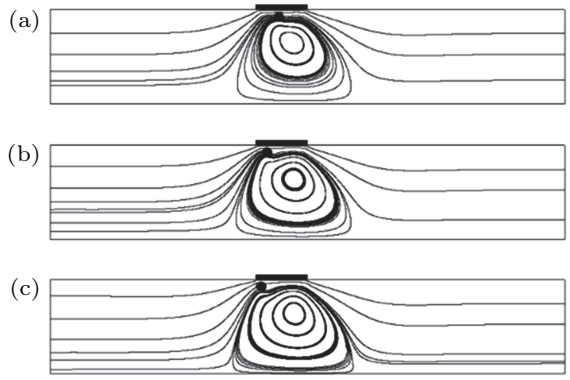


Fig. 12. Schematic diagram of the interaction between a particle and the flow field at initial positions $y_{p0} = 0.25$ (a), 0.5 (b), and 0.8 (c).

Figure 12 displays the effects of a particle on the flow field, when the strongest hydrodynamic force is exerted on this particle. When the particle is released from the $y_p = 0.25$, the interference is weak, as Fig. 15(a) shows. Since a stronger hydrodynamic force is obtained when this particle is released from a higher y_p, the interference is more significant. As shown in Fig. 15(c), as the initial position increases to $y_p = 0.8$, the influence becomes more significant, and the flow field around the particle becomes obviously distorted.

4.4. Effect of particle density

For similar particle volumes, particle mass varies with its density ρ_p. In this subsection, a particle with a radius of 5 μm is released at the initial position ($y_{p0} = 0.5$). When it moves in the flow field ($u_0 = 2 \times 10^{-2}$), its motion varies with its density. As shown in Fig. 13(a), when it is not subjected to an nDEP force, its density is respectively $\rho_p = 0.2$, 1, or 5, and is carried downstream of the channel. Since its velocity decreases more slowly for the particle with higher density, the particle with a higher density approaches to the modulating electrode, and it is closer to the channel wall. When an nDEP force is exerted on the particle, it continues to be carried downstream of the channel when its density is $\rho_p = 0.2$ as seen in Fig. 13(b).

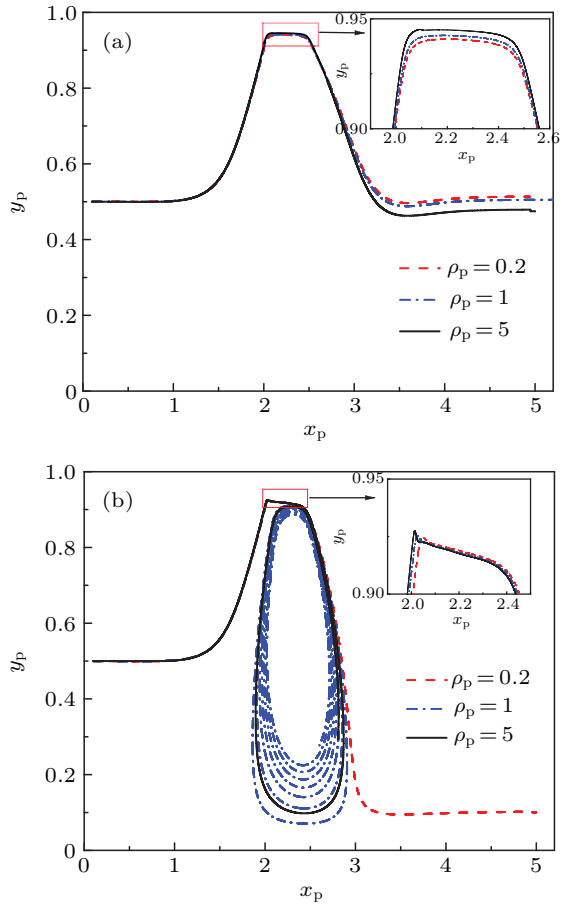


Fig. 13. Trajectories of particle with different densities ρ_p moving with the fluid, for particle subjected to (a) nDEP force and (b) no nDEP force.

However, as its density increases to 1 or 5, the particle is pushed into the vortex by a greater nDEP force, and moves

spirally and toward the center of the vortex. Since the particle has a higher density and can move closer to the modulating electrode, a stronger nDEP force is exerted on this particle as the distance between this particle and the modulating electrode shortens as shown in Fig. 14. In a word, a particle with a higher density is subjected to a stronger nDEP force, so this denser particle can be captured by the vortex more easily.

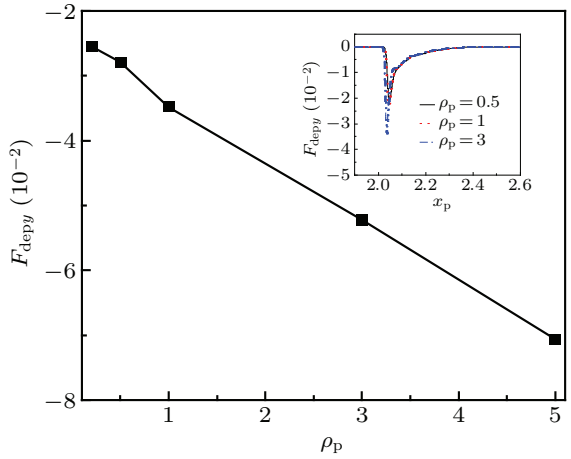


Fig. 14. Variation of nDEP force F_{depy} on particle with density ρ_p when the particle is closest to the modulating electrode.

4.5. Effect of particle size

When particles of different sizes are released from the initial position ($y_{p0} = 0.5$), they move in the flow field ($u_0 = 2 \times 10^{-2}$). As shown in Fig. 15(a), when the particle is not subjected to an nDEP force, it is carried downstream of the channel. However, when an nDEP force is exerted on this particle, small particle is still carried downstream of the channel, but large particle is captured by the vortex. For example, a particle is carried downstream of the channel when its radius is $r = 2.5$ μm, as illustrated in Fig. 15(b). As its radius increases to 5 μm or 10 μm, it is pushed into the vortex by an nDEP force, and moves spirally and toward the center of the vortex. It is pushed closer to the center of the vortex when the radius is $r = 10$ μm. According to Eq. (8), the strength of the DEP force is related to the particle radius, and the nDEP force on the particle becomes stronger as its radius increases as shown in Fig. 16. Thus, large particle is likely to be captured by the vortex.

It follows that a greater hydrodynamic force is generated for a larger particle due to a stronger nDEP force. For the interaction between the particle and the flow field, the influence of a larger particle on the flow field is more significant. When the radius is $r = 2.5$ μm, the change in the flow field is not so large as observed in Fig. 17(a), because the hydrodynamic force is weak. As its radius is $r = 10$ μm, it is subjected to a stronger hydrodynamic force, so the surrounding flow field is significantly distorted as illustrated in Fig. 17(c).

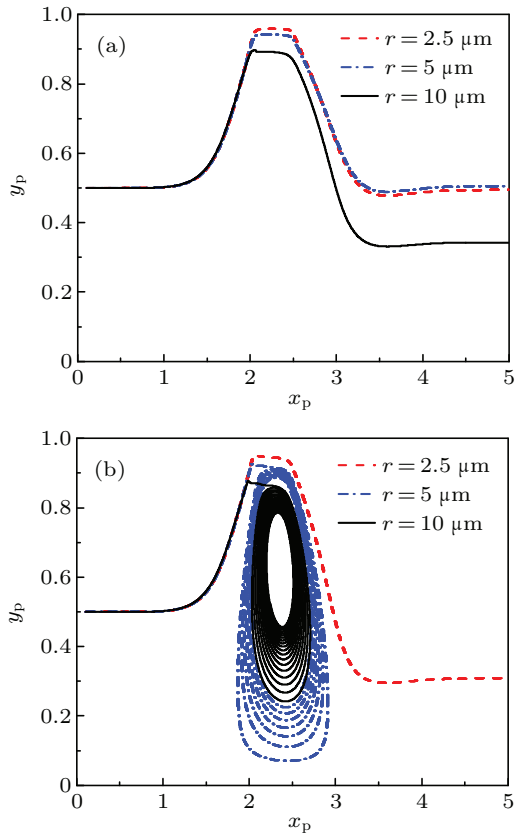


Fig. 15. Schematic diagram of the trajectories of particles with different radii, indicating its trajectories within the channel when (a) subjected to no nDEP force and (b) under action of nDEP force.

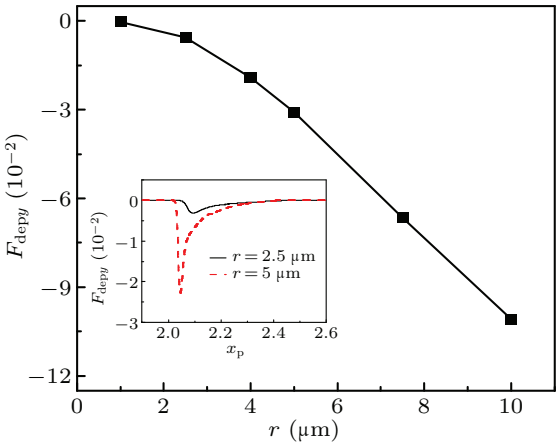


Fig. 16. Variation of nDEP force F_{depy} on particle with particle radius r when moving closest to modulating electrode.

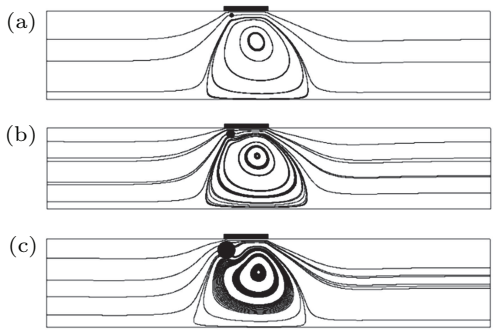


Fig. 17. Schematic diagram of influence of particles of different sizes ((a) $r = 2.5$ μm, (b) $r = 5$ μm, and (c) $r = 10$ μm) on flow field when particles are the closest to the modulating electrode.

4.6. Effect of slip velocity

A particle with a radius of 5 μm is released from the initial position $y_{p0} = 0.5$, and moves with the fluid. When an nDEP force acts on this particle, its motion varies with the slip velocity u_0. As shown in Fig. 18(a), when the particle is not subjected to an nDEP force, it is carried downstream of the channel. When it is subjected to an nDEP force, it can be captured by the vortex when the slip velocity falls below $u_0 = 2 \times 10^{-2}$ as shown in Fig. 18(b).

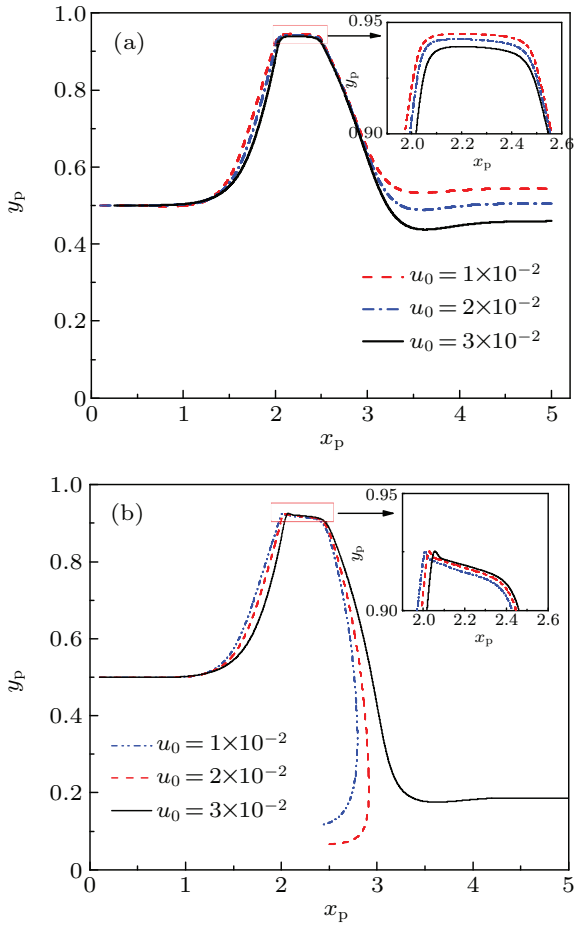


Fig. 18. Trajectories of a particle when moving in a flow field with different values of slip velocities u_0 (a) without and (b) with nDEP force acting on it.

As the slip velocity is higher than $u_0 = 3 \times 10^{-2}$, it is carried downstream along the channel. Moreover, as the particle moves close to the modulating electrode, its position in the x-direction x_p becomes closer to the ending of the modulating electrode as the u_0 increases. However, the value of $(y_p)_{max}$ is approximate. Thus, the nDEP force on this particle is also approximate. Since this particle can pass through the modulating area faster at a greater u_0, the time in which the DEP force acts on this particle t_E is shorter as observed in Fig. 19(b). Accordingly, the particle is more likely to be carried downstream in a high-velocity flow field because it cannot be pushed into the vortex by the nDEP force within the short time t_E. The results show that the ability of the vortex to trap this particle decreases in a high-velocity flow field, which is consistent with the finding of our previous work.[22,38,44]

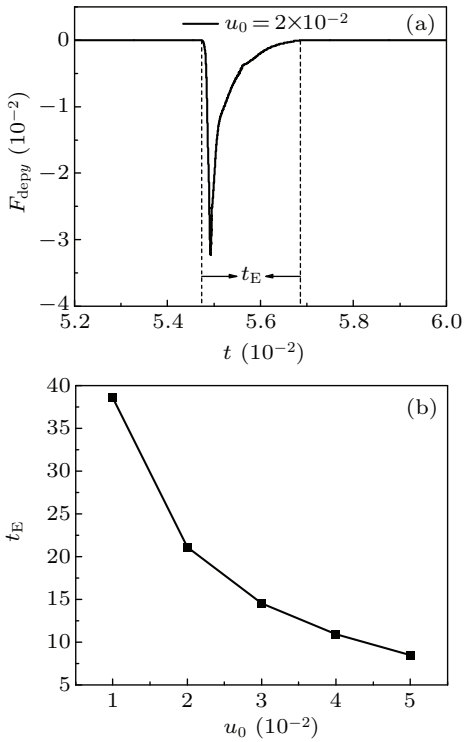


Fig. 19. (a) Variation of nDEP force on particle F_{depy} with time t, and (b) variation of t_E with u_0.

5. Conclusions

In this work, an approach that combines the finite difference method and the lattice Boltzmann method is used to study the interactions between the particle and the flow field in a system that combines the field-modulating vortex and DEP. The particle moves with the fluid within the channel due to the hydrodynamic force. The particle without the nDEP force can be captured by the vortex when the particle is initially placed near the wall due to fluid–particle interactions. However, as the y_{p0} increases, the particle cannot be captured by the vortex and moves downstream in the channel. It is found that when subjected to an nDEP force, the particle may be captured by the vortex over a wider range of parameters. The ability of the vortex to capture particle increases with the nDEP force increasing. Since the particle moves closer to the modulating electrode as the y_{p0} increases, it is more likely to be pushed into the vortex by a stronger nDEP force. Moreover, the ability of the vortex to capture the particle increases with the density of the particle increasing because of a stronger nDEP force acting on the particle as it moves closer to the modulating electrode. Similarly, the particle is more likely to be captured by the vortex when the u_0 is lower or r is larger. Therefore, in practical applications, the y_{p0} is higher and the u_0 is lower, the vortex to capture particle is more favorable. In order to make sure a great efficiency of the system for manipulation of particle,

the y_{p0} and u_0 are $y_{p0} \approx 0.5H$ and $u_0 = 2 \times 10^{-2}$, respectively. The effect of the particle motion on the flow field varies with its position. As a particle moves closer to the channel wall, its effect on the surrounding flow field becomes more significant. In addition, the influence of the particle on the flow field is enhanced with the increase of the size, density, or initial position in the y direction of particle.

Acknowledgement

Project supported by the National Natural Science Foundation of China (Granmt Nos. 11572139, 11872187, and 12072125).

Appendix A: Nondimensionalization of governing equation

A1. Nondimensionalization of governing equation of electric field

By introducing $x^* = x/H$, $y^* = y/H$, $\varphi^* = \Delta\varphi/E_0H$, equation (1) can be normalized as

$$\nabla^{*2}\varphi^* = 0, \tag{A1}$$

where H represents the characteristic length, $E_0 = \Delta\varphi/H = \varphi_1/H$ is characteristic electric strength, and the superscript '*' indicates the dimensionless variables. The corresponding boundary conditions are $\varphi_1^* = 1$ and $\partial\varphi^*/\partial n = 0$, respectively.

When the dimensionless variables $\psi^* = \psi/\psi_0 = \psi/(k_BT/ze)$, $n^{+^*} = n^+/n_0$, $n^{-^*} = n^-/n_0$ and $\rho_e^* = \rho_e/(zen_0)$ are introduced, equations (2)–(4) can be normalized into

$$\nabla^{*2}\psi^* = -\frac{k^2}{2}\rho_e^*, \tag{A2}$$

$$\rho_e^* = n^{+*} - n^{-*}, \tag{A3}$$

$$n^{+*} = \mathrm{e}^{-\psi^*}, n^{-*} = \mathrm{e}^{\psi^*}, \tag{A4}$$

where $k = \sqrt{2z^2e^2n_0/(\varepsilon_f k_B T)}$ is the Debye–Huckel parameter, and its reciprocal is equal to the thickness of characteristic EDL. The Dirichlet boundary condition ψ^* is implemented for the regulating electrode, and the other walls are the Neumann boundary, $\partial\psi^*/\partial n = 0$.

A2. Nondimensionalization of governing equation of particle motion

By introducing the dimensionless variables $m^* = m/m_0$, $F^* = F/F_0$, and $\gamma = 6\pi aE_0/\psi_0$, the characteristic force is $F_0 = \varepsilon_f\varphi_0^2$. Thus equations (7) and (8) can be normalized into

$$m^*\frac{\mathrm{d}^2\boldsymbol{r}_p^*}{\mathrm{d}t^{*2}} = \boldsymbol{F}_{dep}^* + \boldsymbol{F}_d^*, \tag{A5}$$

$$F_{dep}^* = 2\pi a^{*3}\varepsilon_f^* \mathrm{Re}\left[f_{cm}\right]\nabla^*\left|\boldsymbol{E}^*\right|^2. \tag{A6}$$

References

[1] Zhang H, Chang H and Neuzil P 2019 *Micromachines* **10** 423
[2] Hughes M P 2016 *Biomicrofluidics* **10** 032801
[3] Yao J, Zhu G, Zhao T and Takei M 2019 *Electrophoresis* **40** 1166
[4] Alazzam A, Mathew B and Alhammadi F 2017 *J. Sep. Sci.* **40** 1193
[5] Chen X, Ren Y, Liu W, Feng X, Jia Y, Tao Y and Jiang H 2017 *Anal. Chem.* **89** 9583
[6] Wu C, Chen R, Liu Y, Yu Z, Jiang Y and Cheng X 2017 *Lab on a Chip* **17** 4008
[7] Çetin B, Özer M B, Çağatay E and Büyükkoçak S 2016 *Biomicrofluidics* **10** 014112
[8] Wang Y, Wang J, Wu X, Jiang Z and Wang W 2019 *Electrophoresis* **40** 969
[9] Yao J, Obara H, Sapkota A and Takei M 2016 *Biomicrofluidics* **10** 024105
[10] Yao J and Takei M 2017 *IEEE Sens. J.* **17** 8196
[11] Yao J, Sugawara M, Obara H, Mizutani T and Takei M 2017 *IEEE Transactions on Biomedical Circuits and Systems* **11** 1450
[12] Yafouz B, Kadri N A and Ibrahim F 2014 *Sensors (Switzerland)* **14** 6356
[13] Jones P V, Salmon G L and Ros A 2017 *Anal. Chem.* **89** 1531
[14] Lentz C J, Hidalgo-Caballero S and Lapizco-Encinas B H 2019 *Biomicrofluidics* **13** 044114
[15] Rabbani M T, Schmidt C F and Ros A 2017 *Anal. Chem.* **89** 13235
[16] De Pena A C, Redzuan N H M, Abajorga M K, Hill N, Thomas J A and Lapizcoencinas B H 2019 *Micromachines* **10** 450
[17] Zhang J, Yan S, Yuan D, Alici G, Nguyen N T, Ebrahimi Warkiani M and Li W 2016 *Lab on a Chip* **16** 10
[18] Aghaamoo M, Aghilinejad A, Chen X and Xu J 2019 *Electrophoresis* **40** 1486
[19] Sun H, Ren Y, Liu W, Feng X, Hou L, Tao Y and Jiang H 2018 *Anal. Chem.* **90** 11376
[20] Chen X, Ren Y, Hou L, Feng X, Jiang T and Jiang H 2019 *Nanoscale* **11** 6410
[21] Tajik P, Saidi M S, Kashaninejad N and Nguyen N 2020 *Ind. Eng. Chem. Res.* **59** 3772
[22] Xie C, Chen B, Yan B and Wu J 2018 *Appl. Math. Mech.* **39** 409
[23] Teh E J and Johansen C T 2016 *Acta Astronaut.* **128** 431
[24] Crowe C, Troutt T and Chung J 1995 *Particle Interactions with Vortices* (Fluid Mechanics and Its Applications) pp. 829–861
[25] Tio K K, Lasheras J C, Linan A and Gañán-Calvo A M 1993 *J. Fluid Mech.* **254** 671
[26] Raihan M K, Li D, Kummetz A J, Song L, Yu L and Xuan X 2020 *Appl. Phys. Lett.* **116** 183701
[27] Volpe A, Gaudiuso C and Ancona A 2019 *Micromachines* **10** 594
[28] MacH A J, Kim J H, Arshi A, Hur S C and Di Carlo D 2011 *Lab on a Chip* **11** 2827
[29] Zhou J, Kasper S and Papautsky I 2013 *Microfluid. Nanofluid.* **15** 611
[30] Shen F, Xu M, Wang Z and Liu Z M 2017 *Appl. Phys. Express* **10** 097301
[31] Shen F, Li Z, Xue S, Li M and Liu Z 2021 *J. Phys. D: Appl. Phys.* **54** 025401
[32] Haddadi H and Di Carlo D 2017 *J. Fluid Mech.* **811** 436
[33] Qiao J, Deng R and Wang C H 2015 *Int. J. Multiphase Flow* **77** 120
[34] Chao K, Chen B and Wu J 2010 *Biomed. Microdevices* **12** 959
[35] Mirbozorgi S, Niazmand H and Renksizbulut M 2006 *J. Fluids Eng.* **128** 1133
[36] Cetin B and Li D 2008 *Electrophoresis* **29** 994
[37] Li M, Li W, Zhang J, Alici G and Wen W 2014 *J. Phys. D: Appl. Phys.* **47** 063001
[38] Yan B, Chen B, Liu F, Wu J and Xiong Y 2021 *Appl. Math. Mech.* **42** 371
[39] Li H, Lu X, Fang H and Qian Y 2004 *Phys. Rev. E* **70** 026701
[40] Tang G H, Li Z, Wang J K, He Y L and Tao W Q 2006 *J. Appl. Phys.* **100** 094908
[41] Lallemand P and Luo L S 2003 *J. Comput. Phys.* **184** 406
[42] Bouzidi M, Firdaouss M and Lallemand P 2001 *Phys. Fluids* **13** 3452
[43] Mei R, Yu D, Shyy W and Luo L S 2002 *Phys. Rev. E* **65** 041203
[44] Yan B, Chen B, Xing Y L and Peng Z R 2021 *Chin. Phys. B* **30** 114701